2023 IEEE International Conference on Robotics and Automation (ICRA 2023)
May 29 - June 2, 2023. London, UK

Morphological Characteristics That Enable Stable and Efficient Walking in Hexapod Robot Driven by Reflex-based Intra-limb Coordination

Wataru Sato[1], Jun Nishii[2], Mitsuhiro Hayashibe[1], and Dai Owaki[1]

Abstract— **Insects exhibit adaptive walking behavior in an unstructured environment, despite having only an extremely small number of neurons (10^5 to 10^6). This suggests that not only the brain nervous system but also properties of the physical body, such as the morphological characteristics, play an essential role in generating such adaptive behavior. Our study aims at investigating the effect of body morphological characteristics on the walking performance in a robot model, which is designed to mimic an insect. To this end, we constructed an insect-like hexapod model in a simulation environment that implements a reflex-based intra-limb coordination control. Herein, for a set of walking parameters, which were optimized to maximize the energy efficiency at the target speed, we investigated the effects of changes in the standard posture of the two leg joints on the walking success rate for various initial conditions and cost of transport (CoT) as an index of energy efficiency. Simulation results indicated that robots with specific morphological characteristics similar to those of insects exhibited high gait stability and energetic efficiency. Because only the reflex-based control was employed, the inter-leg coordination occurred spontaneously, suggesting that our approach would lead to a useful design methodology from the perspective of computational cost in generating the walking locomotion.**

I. Introduction

Compared to wheeled robots, Legged robots have an excellent ability to traverse uneven terrain [1], and therefore, are expected to perform successfully in tough and challenging environments, such as disaster sites and off-planet terrain [2], [3]. In particular, among legged robots, hexapod robots have outstanding walking stability and fault tolerance; however, owing to the large number of degrees of freedom (DoFs), it is challenging to design the control laws that coordinate the leg movements. To overcome this issue, several studies have attempted to control hexapod robots inspired by gait generation mechanism of insects [4]–[6]. Compared to other animal species, insects have a much smaller number of neurons [7], [8]; However, they are capable of exhibiting flexible gait patterns by coordinating the inter- and intra-limb DoFs according to the situation [9]–[11]. Furthermore, in the case where one leg or a few legs have been amputated, insects can continue walking through the adaptive inter- and intra-limb coordination by exploiting the remaining legs [12]–[14]. Therefore, the development of a hexapod robot with walking functionality comparable to insects will contribute to the elucidation of the leg coordination mechanism of insects.

Biological findings suggest that the inter- and intra-limb coordination, which is responsible for the adaptive locomotion generation in insects is largely controlled in a decentralized manner by the neural networks located in thoracic ganglia [15]–[18]. Based on these findings, studies have attempted to reproduce insect gait patterns by modeling a neural network called a *Central Pattern Generator (CPG)* [19], which generates autonomous periodic control commands, or a *chain of reflexes* [20], which generate movement based on only the sensory input without autonomous neural activities. In CPG-based approaches [5], [19], [21], [22], [24]–[26], a control system was modeled using the coupled or decoupled oscillators to generate feedforward motor commands with sensory feedback to the controllers. In chain-of-reflex approaches [20], [27]–[30], a control system was modeled using many chained discontinuous reflexive events, in which locomotion can be generated purely from the interaction between the sensory feedback signals and the body. Using these models, various functions that closely resemble the walking ability of insects are being verified through numerical simulation and/or robotic experiments ([31], [32], and reviewed in [6]).

Although these studies have primarily focused on neural control mechanism for gait generation, the functional role of body morphology is a crucial aspect associated with the ability of insects to adapt their simple and limited neural architecture to diverse environments [33], representing the *embodiment* concept [34]. However, few studies have discussed the effects of body morphology in detail, which is essential for functional emergence, on gait performance: the effect of toe adhesion on gait in *Drosophila* model [35]; the reproduction of gait and ball rolling based on leg morphology in a dung beetle model [36], [37]; and a smooth and efficient mobile robot inspired by function of beetle claw [38].

This study aims to verify the effect of morphological characteristics of a hexapod robot on its walking performance. As a morphological characteristic of the hexapod robot, we focused on the standard posture of the legs relative to the body segment. To verify the effect, we modeled a hexapod robot with a simple controller, that is, a reflex-based intra-limb coordination control [39] on a simulator and conducted a walking simulation. We used the success rate of walking from various initial conditions and Cost of Transport (CoT) [40], a measure of energy efficiency, as evaluation indices of walking performance. We found that the walking performance improved when the second leg joint (J_2 joint

This work was supported by a JSPS KAKENHI Grant-in-Aid for Scientific Research on Innovative Areas through the Project "Science of Soft Robot" under Grant JP21H00317, JP18H03167, and JP20H04260.

[1]WS, MH, and DO are with the Neuro-Robotics Lab, Department of Robotics, Graduate School of Engineering, Tohoku University, Sendai 980-8579, Japan. owaki@tohoku.ac.jp

[2]JN is with the Graduate School of Sciences and Technology for Innovation, Yamaguchi University, Yamaguchi, 753-8512, Japan.

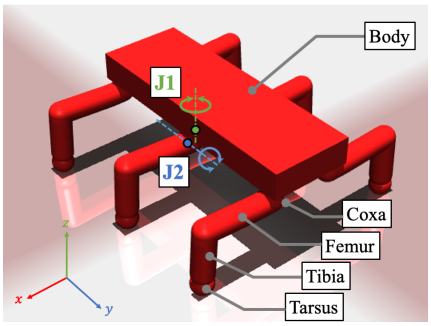

(a) Overview

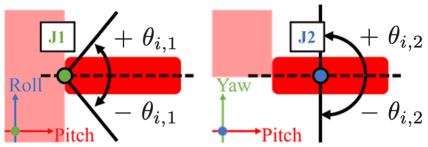

(b) Rotational range of J_1 and J_2 joints around their axes.

Fig. 1: Hexapod robot model developed in simulation.

TABLE I: Parameters for Hexapod Robot Model

Segment (Shape)	Mass	Height/Radius	Length	Width
Body (Box)	4.0 [g]	10.0 [mm]	90 [mm]	30[mm]
Coxa (Capsule)	40.0 [mg]	4.0 [mm]	6 [mm]	—
Femur (Capsule)	36.0 [mg]	4.0 [mm]	20 [mm]	—
Tibia (Capsule)	20.0 [mg]	4.0 [mm]	16 [mm]	—
Tarsus (Sphere)	4.0 [mg]	4.0 [mm]	—	—

in Fig.1) was set in the upper position and the first joint (J_1 joint in Fig.1) of the fore, middle, and hind legs was set in the forward, backward, and backward position in the standard posture, respectively.

II. Method

A. Hexapod Robot Model

The hexapod robot (Fig. 1 (a)) used in walking simulation was constructed based on the parameters of the cockroach (*Blaberus discoidalis*) measured by Kram et al. [41] in Table I. The body of insects consists of head, thorax, and abdomen, and each leg consists of five segments: coxa, trochanter, femur, tibia, and tarsus [41]. The hexapod robot employed in this study consists of a body with six legs ($i = 1,\ldots,6$), each of which has four segments excluding the trochanter, as shown in Fig. 1 (a). Although the joints in the body segments have been reported to be effective in climbing [42], in this study the body was composed of a single rigid body for design simplicity. Each leg has two joints ($j = 1,2$): a yaw-axis joint between the body and coxa (J_1) and a roll-axis joint between the coxa and femur (J_2). Each of them have one degree of freedom. The rotational range of J_1 and J_2 are $\pm\pi/4$ rad (front and back) and $\pm\pi/2$ rad (up and down), respectively (Fig. 1 (b)). The right front (RF), right middle (RM), right hind (RH), left front (LF), left middle (LM), and left hind (LH) legs are denoted as R1, R2, R3, L1, L2, and L3, respectively.

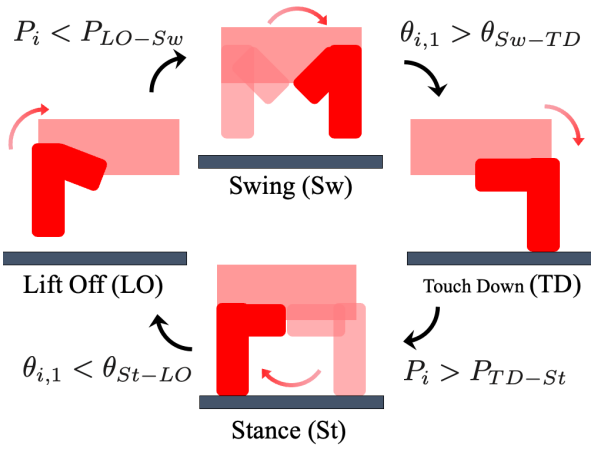

Fig. 2: Reflex-based Intra-limb Coordination Control.

TABLE II: Parameter Ranges for Optimization

State	Torque	Min	Max	Parameters	Min	Max
Sw	$\tau_{i,1}^{Sw}$ [Nmm]	0.0	8.0	θ_{Sw-TD} [rad]	0	$\pi/4$
Sw	$\tau_{i,2}^{Sw}$ [Nmm]	0.0	8.0	P_{TD-St} [mN]	0.0	5.0
TD	$\tau_{i,1}^{TD}$ [Nmm]	-8.0	8.0	θ_{St-LO} [rad]	-$\pi/4$	0
TD	$\tau_{i,2}^{TD}$ [Nmm]	-8.0	0.0	P_{LO-Sw} [mN]	0.0	5.0
St	$\tau_{i,1}^{St}$ [Nmm]	-8.0	0.0	k_1 [Nmm/rad]	0.0	8.0
St	$\tau_{i,2}^{St}$ [Nmm]	-8.0	0.0	c_1 [s]	0.01	0.1
LO	$\tau_{i,1}^{LO}$ [Nmm]	-8.0	8.0	k_2 [Nmm/rad]	0.0	8.0
LO	$\tau_{i,2}^{LO}$ [Nmm]	0.0	8.0	c_2 [s]	0.01	0.1

B. Reflex-based Intra-limb Coordination Control

The walking control of the hexapod robot used in our study is based on the reflex-based intra-limb coordination control [39] inspired by Ekeberg's model [43]. The hexapod robot model walks by actuating two joints of each leg, with the J_1 joint moving the leg forward and backward and the J_2 joint moving the leg up and down to lift it off the ground or ground it. The reflex-based intra-limb coordination (Fig. 2) performs walking motion by transitioning between the following four states: (i) Swing (Sw) to move the leg forward; (ii) Touch Down (TD) to ground the leg; (iii) Stance (St) to support the body; and (iv) Lift Off (LO) to lift the leg off the ground. To simplify the control law, in each state, the torque $\tau_{i,1}$ and $\tau_{i,2}$ are kept constant. Table II shows the search range of constant torque inputs $(\tau_{i,1}, \tau_{i,2})$ for J_1 and J_2 joints in each state to be optimized in Section II-D.

The transition between each state is reflexively achieved when the sensory input satisfies the following conditions (Fig. 2): (i) Transition from Sw to TD is achieved when the J_1 joint angle $\theta_{i,1}$ increases beyond a threshold value θ_{Sw-TD}; (ii) From TD to St is achieved when the load (foot pressure) on the leg P_i increases beyond a threshold value P_{TD-St}; (iii) From St to LO is achieved when the J_1 joint angle $\theta_{i,1}$ becomes less than a threshold value θ_{St-LO}; and (iv) From LO to Sw is achieved when the foot pressure P_i becomes less than a threshold value P_{LO-Sw}. Table II shows the search range of the threshold values $(\theta_{Sw-TD}, P_{TD-St}, \theta_{St-LO}, P_{LO-Sw})$ for the state-transitions to be optimized in Section II-D.

C. Joint Stiffness

Muscles and exoskeleton contribute to the elastic component. Their restorative force has been reported to contribute to the leg movements in insects while performing the walking motion [44]. Furthermore, in this study, since the walking was generated by torque inputs from reflex-based intra-limb coordination control, joint motion was limited to the predefined angle range. Herein, we implemented the passive elastic elements at each leg joint to limit the range of motion by joint stiffness. The torque $\tau_{i,j}^{stiff}$ generated by the elastic elements, i.e., mechanical spring and damper, was calculated by the following equation:

$$\tau_{i,j}^{stiff}(t) = -k_j\{\theta_{i,j}(t) - \theta_{0,j}\} - k_j c_j \dot{\theta}_{i,j}(t), \quad (1)$$

where k_j is the elastic coefficient, c_j is the viscosity coefficient, $\theta_{i,j}$ is the joint angle, and $\dot{\theta}_{i,j}$ is the joint angular velocity. $\theta_{0,j}$ denote the standard posture of each joint (j =1 or 2). The sum of the input torque by the reflex-based control and the elastic torque generated by (1) constitute the total torque input to each joint. Table II shows the search range of the coefficient (k_1, c_1, k_2, c_2) for the joint stiffness to be optimized in Section II-D.

D. Parameter Optimization

For the simulation, we used the physics simulator MuJoCo [46]. The collision model implemented in Mujoco accurately models contact and repulsive forces between objects with complex shapes, taking into account their shape, size, and material properties. The algorithm incorporates the flexibility to allow for the precise simulation of contact and reaction forces. The parameters shown in Table II were optimized using Optuna (Preferred Networks, [45]), a python library capable of performing Bayesian optimization. For the evaluation function, we used (2), which is the product of a normal distribution around the target velocity and CoT (Cost of Transport) (3) as an index of energy efficiency:

$$\varepsilon^{-1} = \mathrm{CoT} \cdot \frac{1}{\sqrt{2\pi\sigma^2}} \exp\left\{\frac{(v-\bar{v})^2}{2\sigma^2}\right\} \quad (2)$$

$$\begin{aligned} \mathrm{CoT} &= \frac{\Sigma_{i,j} e_{i,j}}{MD}, \quad (3) \\ e_{ij} &= \int_T^{T'} \left(\delta(\dot{\theta}_{i,j}(t)\tau_{i,j}(t)) + \gamma\tau_{i,j}^2(t)\right) dt, \\ \delta(x) &= \begin{cases} x & (x > 0) \\ 0 & (x \leq 0) \end{cases}, \end{aligned}$$

where $\dot{\theta}_{i,j}$ is the angular velocity of the joint, $\tau_{i,j}$ is the joint input torque, T is the evaluation start time, T' is the evaluation end time, γ $(= 0.005)$ is a constant value that determines the maximum efficiency of the actuator [47], M is the total robot weight, v is the measured robot velocity, $\bar{v}$ is the target velocity, and σ $(= 0.01)$ is the standard deviation for the normal distribution. Optimization was performed to simultaneously reduce the difference between the target and measured velocities and the CoT. For the travel distance D, the linear distance from the initial position was used for optimization, and the total distance traveled was used for the post-optimized gait evaluation. In the optimization, the walking parameters were updated 10,000 times (one trial of robot walking for 60 s).

TABLE III: Optimized Parameters for Hexapod Model

Parameters	Values	Parameters	Values
$\tau_{i,1}^{Sw}$ [Nmm]	2.12	θ_{Sw-TD} [rad]	2.99×10^{-1}
$\tau_{i,2}^{Sw}$ [Nmm]	2.62	P_{TD-St} [mN]	1.83×10^{-1}
$\tau_{i,1}^{TD}$ [Nmm]	-0.67	θ_{St-LO} [rad]	-2.37×10^{-2}
$\tau_{i,2}^{TD}$ [Nmm]	-0.97	P_{LO-Sw} [mN]	4.76×10^{0}
$\tau_{i,1}^{St}$ [Nmm]	-1.07	k_1 [Nmm/rad]	5.11×10^{0}
$\tau_{i,2}^{St}$ [Nmm]	-0.65	c_1 [s]	1.22×10^{-2}
$\tau_{i,1}^{LO}$ [Nmm]	0.86	k_2 [Nmm/rad]	7.84×10^{0}
$\tau_{i,2}^{LO}$ [Nmm]	1.26	c_2 [s]	4.90×10^{-2}

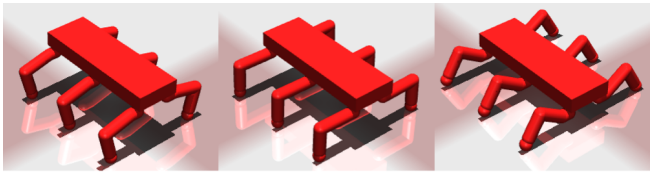

$\theta_{0,2} = -\pi/12$ rad $\quad \theta_{0,2} = 0.0$ rad $\quad \theta_{0,2} = \pi/6$ rad

Fig. 3: Changes in morphological characteristics due to different standard postures of J_2 joints.

E. Evaluation of Optimization Results

The walking motion performed by the robot was evaluated for 300 s using the optimized parameters. The walking performance was evaluated based on the CoT calculated using (3) and the success rate of walking from various initial conditions (100 conditions). One of the four walking states (Sw, TD, St, LO) was randomly assigned to each of the six legs as the initial condition. For all the simulations, the control parameters were the same except for the physical parameters that characterize the morphological characteristics of the robot body. The robot was considered to have failed in performing the walking motion if the robot fell down, or if one of the legs did not transition to the next walking state for a certain period of time (1.5 s).

III. Simulation Results

A. Optimization Results

The walking parameters were optimized over five trials with a target velocity of 0.4 m/s with $\theta_{0,1} = \theta_{0,2} = 0$ rad for all legs. For evaluation, the parameters with the highest energy efficiency (lowest CoT) out of the five trials were used. The parameters obtained after the optimization are shown in Table III. In our study, these parameters were used as a baseline to verify the effect of the standard posture.

B. Effect of standard posture of J_2 joints

We performed walking simulations by changing the standard posture $\theta_{0,2}$ of J_2 (Fig. 3) in the range from $-\pi/4$ to $\pi/4$ rad (in $\pi/36$ rad interval). Figure 4 shows the

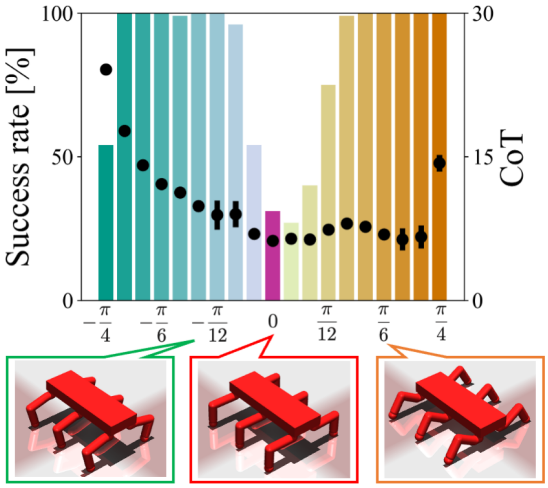

Fig. 4: Succes rate and CoT for each J_2 condition.

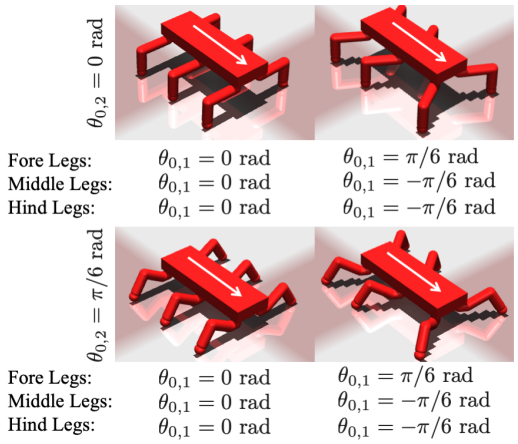

Fig. 5: Changes in morphological characteristics due to different standard postures of J_1 joints.

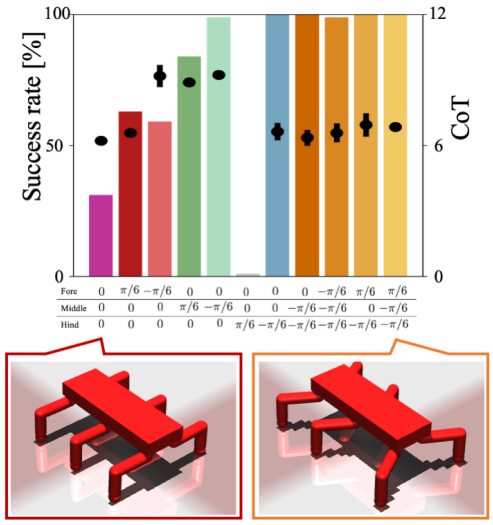

(a) $\theta_{2,0} = 0.0$ rad

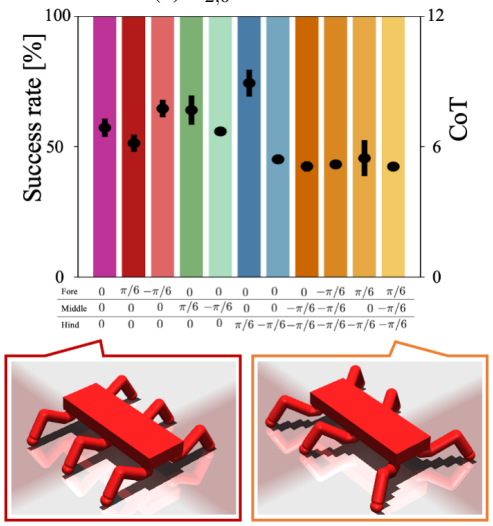

(b) $\theta_{2,0} = \pi/6$ rad

Fig. 6: Succes rate and CoT for each J_1 condition.

corresponding results, where the bars and black dots indicate the success rate and CoT (mean and SD), respectively. The CoT tended to increase as the angle $\theta_{0,2}$ of J_2 became smaller than 0 rad, while the CoT kept as low as $\theta_{0,2}$=0 where $\theta_{0,2} > 0$, except for the case of $\pi/4$ rad.

C. Effect of standard posture of J_1 joints

As shown in Fig. 5, the simulation was conducted under conditions wherein the J_1 standard posture $\theta_{0,1}$ was varied forward and backward ($\pm\pi/6$ rad). Figure 6 (a) shows the results in response to the J_1 standard posture $\theta_{0,1}$ when the J_2 standard posture $\theta_{0,2} = 0$ rad. The different colors of the bars indicate the different J_1 conditions, for example, the magenta color condition means $\theta_{0,1} = 0$ for all front, middle, and hind legs, while the yellow color condition means $\theta_{0,1} = \pi/6$ for the front legs, $\theta_{0,1} = -\pi/6$ for the middle, and $\theta_{0,1} = -\pi/6$ for the hind legs. The results for front, middle, and hind legs with varying J_1 standard posture $\theta_{0,1}$ showed that the success rate of walking was higher when the J_1 angle was set backward ($\theta_{0,1} = -\pi/6$ rad) for the hind legs (sky blue and yellow colors). There was no trend in CoT according to the standard posture of J_1. As shown in Fig. 6 (b), when $\theta_{0,2} = \pi/6$ rad, the walking success rate remained 100% in all the conditions. The CoT was lower when the standard posture $\theta_{0,1}$ of J_1 was set backward ($-\pi/6$) for the hind legs (sky blue and yellow colors).

D. Generated Gaits

Figure 7 shows the tarsus trajectories and gait diagrams (colored region represents St states for each leg from 50.0 to 51.0 s) of representative tetrapod-like steady gaits generated from each morphology. In Fig. 7 (a), the tarsus trajectory becomes smaller when $\theta_{0,2} < 0$ but larger when $\theta_{0,2} > 0$. In Fig. 7 (b), the range of the tarsus trajectories change according to the parameter set of $\theta_{0,1}$ for each leg. This suggests that the change in the tarsus trajectory caused changes in the walking success rate and CoT.

IV. Discussion

Figures 8 (a) and (b) show snapshots of the walking motion during one cycle when $\theta_{0,2} = 0$ rad and $\theta_{0,2} = -\pi/12$

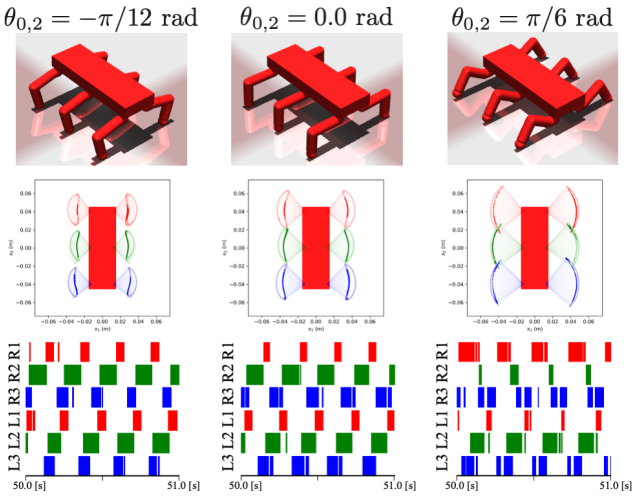

(a) $\theta_{0,1} = 0$ rad for all legs.

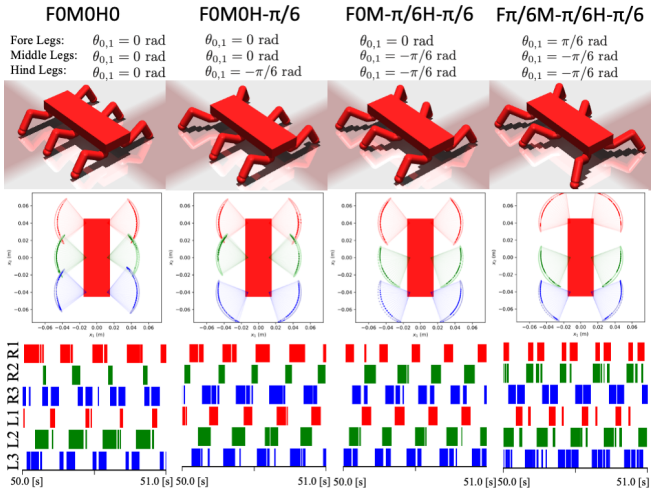

(b) $\theta_{0,2} = \pi/6$ rad for all legs.

Fig. 7: Morphological characteristics (top), tarsus trajectories (middle), and Gait diagram (bottom) for each $(\theta_{0,1}, \theta_{0,2})$.

rad ($\theta_{0,1} = 0$ rad for all legs). The gray area represents the support polygon (the polygon connecting the points where the leg tips are in contact with the ground). In Fig. 8 (a), the robot fell over after the body posterior made contact with the ground. From the same figure, it can be observed that the motions of the left and right front, middle, and hind legs are synchronized. The synchronization of the stance phase of the legs propagated from the front leg with $T = 0.0$ to the middle leg with $T = 0.1$ and the hind leg with $T = 0.5$, in turn. The reflex-based intra-limb coordination control used in this study automatically transitions the walking state from St to LO, St to Sw, and St to TD when the legs are off the ground with satisfying the threshold value. Therefore, when the body tilts backward to some extent and the legs enter the Sw state, the walking state of the legs synchronizes with the other side and the robot tended to fall over, resulting in the lower walking success rate for initial conditions.

On the other hand, we concluded that the higher walking success rate when $\theta_{0,2}$ was smaller than 0 is attributed to the

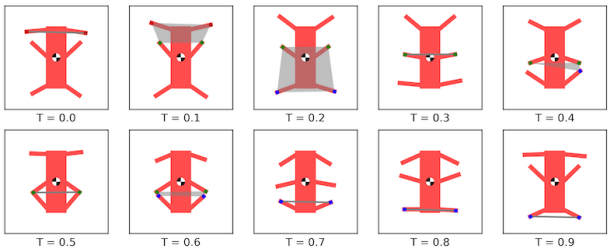

(a) $\theta_{0,2} = 0$ rad, one gait cycle just before the fall.

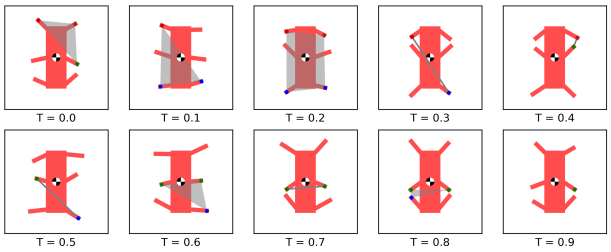

(b) $\theta_{0,2} = -\pi/12$ rad, one gait cycle during steady walking.

Fig. 8: Change in support polygon in the gait snapshot due to J_2 standard posture $\theta_{0,2}$ change, where T was the normalized time in a gait cycle. The simulation was initiated from the same initial conditions. $\theta_{0,1} = 0.0$ rad for all legs.

smaller range of the tarsus trajectory, as shown in Fig. 7 (a) left, and the phenomenon of overlapping of the middle and hind leg tarsus to form a rotation axis did not occur as in Fig. 8 (a) when $T = 0.5$. Additionally, the postural stability was improved as the displacement of the tarsus trajectory in the z-axis direction in 3D space became smaller as $\theta_{0,2}$ became more distant than 0. Although the gait stability was improved, the locomotion velocity decreased as the range of the tarsus trajectories became smaller during one gait cycle, resulting in a higher CoT.

Figure 9 indicates the time evolution of the roll and pitch angles of the robot body for (a) $\theta_{0,2} = 0$ rad; (b) $\theta_{0,2} = \pi/6$ rad; and (c) $\theta_{0,2} = \pi/4$ rad. In the case of Fig. 9 (a) ($\theta_{0,2} = 0$ rad), when the pitch angle of the body exceeded $\pi/4$ rad, contact between the ground and the coxa was observed. The contact in such a large body tilt may have led to the robot fall, resulting in the decrease in the walking success rate (Fig. 4). In Fig. 9 (b) ($\theta_{0,2} = \pi/6$ rad), the pitch angle changes within a range smaller than $\pi/12$ rad (ground-coxa contact was observed at the peak of the pitch angle), suggesting that the small range of pitch angle variation contributed to the improvement in walking success rate with lower CoT (Fig. 4). On the other hand, in Fig. 9 (c) ($\theta_{0,2} = \pi/4$ rad), more frequent contact between the ground and coxa can be observed: the frequent contact causes a large energy loss during walking, suggesting that the propulsive force was insufficient for locomotion. This resulted in a shorter distance traveled in relation to the energy consumption followed by an increase in CoT (Fig. 4).

When the standard posture $\theta_{0,1}$ of J_1 of the fore, middle, and hind leg was changed independently, the highest walking success rate was observed when $\theta_{0,1} = -\pi/6$ of the hind

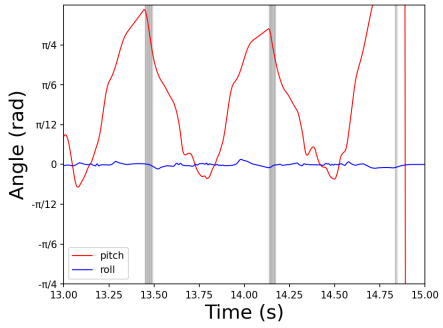

(a) $\theta_{0,2} = 0$ rad

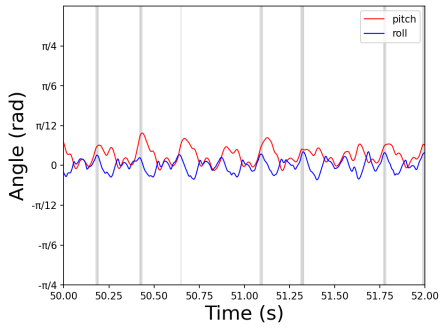

(b) $\theta_{0,2} = \pi/6$ rad

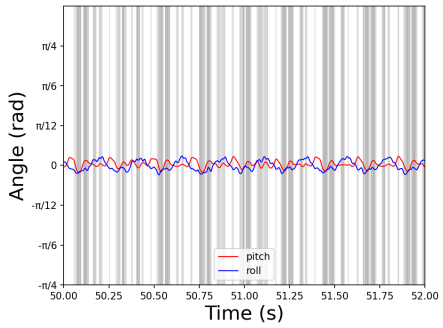

(c) $\theta_{0,2} = \pi/4$ rad

Fig. 9: Time evolution of the roll and pitch angles of the robot body. The gray areas indicate the time periods when the coxa of R1, R3, L1, and L3 (four corners of the body) were in contact with the ground.

leg (Fig. 6 (a)). As shown in Fig. 7 (b), the range of the hind leg motion shifts backward to suppress the pitch angle rotation of the body. In the TD and St walking states, where pushing torque is applied to the ground, the legs are located in front of the body, and thus, tend to fall backward. Therefore, positioning the hind legs backward is effective in maintaining the whole-body balance and preventing the body from falling.

Under the condition that $\theta_{0,2} = 0$ rad and J_1 of the hind leg was tilted in the backward direction $\theta_{0,1} = -\pi/6$ rad, the robot was able to continue walking without making contact with the ground (not shown in Fig. 9). Similarly, the robot walked without contact between the coxa and the ground (no gray area in Fig. 10) in the condition where $\theta_{0,2} = \pi/6$ rad and $\theta_{0,1} = -\pi/6$ rad for the hind legs. In addition, in this case, the high energy efficiency (lower CoT, Fig.6 (b)) may be attributed to the smaller rotation of the pitch angle,

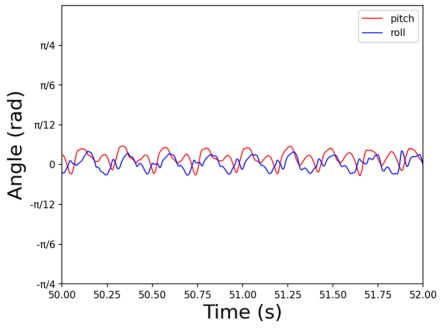

Fig. 10: Time evolution of the roll and pitch angles of the robot body. $\theta_{0,2} = \pi/6$ and $\theta_{0,1} = -\pi/6$ for hind legs.

which reduced the variation of the tarsus trajectory in the z-direction and thus increased the distance traveled in the x-y coordinates.

This study did have some limitations, however. For example, we generally use servo motors as actuators of robots, but the weight and inertia of the motor affect the dynamical motion of the robot legs. On the other hand, the skeletal system of an insect is very light-weight and its muscles have an ideal power-to-weight ratio. Thus, the challenge is to verify a control mechanism that takes into account the physical characteristics of the actuators for robotic applications.

V. Conclusion

By changing the standard postures of the J_1 and J_2 joints of the hexapod robot, we confirmed that the walking success rate and the walking efficiency CoT were improved. In particular, increasing the J_2 joint standard posture $\theta_{0,2}$ above 0 rad enabled us to maintain a high walking success rate while maintaining an energy-efficient CoT. Additionally, by changing the J_1 standard posture of the hind leg backward $\theta_{0,1} = -\pi/6$, we confirmed that the robot achieves high walking success rate and high energy-efficient (low CoT) walking performance. Our findings correspond to the following: (1) the body structure of the cockroach [41], [48], in which the fore legs are directed forward, while the middle/hind legs are directed backward; and (2) the role of each leg during walking in stick insects [49], in which the fore/hind legs generate braking/propulsive forces. The results suggest that a combination of a simple reflex-based intra-limb coordination control and morphological characteristics of the body can achieve walking motion with a high success rate and energy-efficiency. The fact that walking was achieved without any inter-leg coordination control suggests that our approach may have high applicability to real physical robots even from the viewpoint of computational cost.

References

[1] G. Carbone and M. Ceccarelli. "Legged Robot System," Cutting Edge Robotics, IntechOpen, 2005.

[2] J. Bares, M. Hebert, T. Kanade, E. Krotkov, T. Mitchell, R. Simmons, and W. Whittaker. "Ambler: An autonomous rover for planetary exploration," Computer, vol. 22, pp. 18–26, 1989.

[3] A. Preumont, P. Alexandre, I. Doroftei, and F. Goffin. "A conceptual walking vehicle for planetary exploration," Mechatronics, vol. 7, pp. 287–296, 1997.

[4] K. S. Espenschied, R. D. Quinn, R. D. Beer, and H. J. Chiel. "Biologically based distributed control and local reflexes improve rough terrain locomotion in a hexapod robot," Robotics and Autonomous Systems, vol. 18, pp. 59–64, 1996.

[5] P. Arena, L. Fortuna, M. Frasca, and L. Patané. "A cnn-based chip for robot locomotion control," IEEE Transactions on Circuits and Systems I, vol. 52, pp. 1862–1871, 2005.

[6] P. Manoonpong et al. "Insect-inspired robots: Bridging Biological and Artificial Systems," Sensors, vol.21, pp. 7609, 2021.

[7] A.-S. Chiang et al. "Three-dimensional reconstruction of brain-wide wiring networks in drosophila at single-cell resolution," Current biology, vol. 21, pp. 1–11, 2011.

[8] A. P. Alivisatos et al. "The brain activity map project and the challenge of functional connectomics," Neuron, vol. 74, pp. 970—974, 2012.

[9] D. M. Wilson. "Insect walking," Annual review of entomology, vol. 11, pp. 103–122, 1966.

[10] R.E. Ritzmann and A. Büschges. "Adaptive motor behavior in insects," Current Opinion in Neurobiology, vol. 17, pp. 629-–636, 2007.

[11] V. Dürr et al., "Motor flexibility in insects: Adaptive coordination of limbs in locomotion and near-range exploration." Behavioral Ecology and Sociobiology, vol. 72, 2018.

[12] G. H. Hughes. "The co-ordination of insect movements." Journal of Experimental Biology, vol. 34, pp. 306–333, 1957.

[13] M. Grabowska, E. Godlewska, J. Schmidt, and S. Daun-Gruhn. "Quadrupedal gaits in hexapod animals -inter-leg coordination in free-walking adult stick insects." Journal of Experimental Biology vol. 215, no. 24, pp. 4255–4266, 2012.

[14] D. Owaki, H. Aonuma, Y. Sugimoto, and A. Ishiguro, "Leg amputation modifies coordinated activation of the middle leg muscles in the cricket Gryllus bimaculatus," Scientific Reports, vol. 11, no.1, pp. 1327, 2021.

[15] K. G. Pearson and J. F. Iles. "Nervous mechanisms underlying intersegmental co-ordination of leg movements during walking in the cockroach," Journal of Experimental Biology, vol. 58, no.3, pp.725–744, 1973.

[16] U. Bässler and U. Wegner. "Motor output of the denervated thoracic ventral nerve cord in the stick insect carausius morsus," Journal of Experimental Biology, vol. 105, pp. 127–145, 1983.

[17] J. Dean. "Leg coordination in the stick insect carausis morosus: effect of cutting thoracic connectives," Journal of Experimental Biology vol. 145, no.1, pp. 103–131, 1989.

[18] A. Brekowitz and G. Laurent. "Central generation of grooming motor patterns and interlimb coordination in locusts," Journal of Neuroscience, vol. 16, no. 24, pp. 8079–8091, 1996.

[19] R. D. Beer, R. D. Quinn, H. J. Chiel, and R .E. Ritzmann, R. E., "Biologically inspired approaches to robotics: what can we learn from insects?," Communications of the ACM vol. 40, no. 3, pp. 33–38, 1997.

[20] H. Cruse et al. "Walknet - a bioinspired network to control six-legged walking." Neural Networks, vol. 11, pp. 1435–1447, 1998.

[21] R. E. Ritzmann, R. D. Quinn, and M. S. Fischer. "Convergent evolution and locomotion through complex terrain by insects, vertebrates and robots." Arthropod Structure and Development, vol. 33, no. 3, pp. 361–379, 2004.

[22] W. Chen, G. Ren, J. Zhang, and J. Wang, "Smooth transition between different gaits of a hexapod robot via a central pattern generators algorithm." Journal of Intelligent & Robotic Systems, vol. 67, no. 3, pp. 255–270, 2012.

[23] Y. Ambe, T. Nachstedt, P. Manoonpong, F. Wörgotter, S. Aoi, and F. Matsuno. "Stability analysis of a hexapod robot driven by distributed nonlinear oscillators with a phase modulation mechanism," in IEEE/RSJ International Conference on Intelligent Robots and Systems (Tokyo), pp. 5087–5092, 2013.

[24] P. Manoonpong, U. Parlitz, and F. Wörgötter. "Neural control and adaptive neural forward models for insect-like, energy-efficient, and adaptable locomotion of walking machines," Frontiers in Neural Circuits, vol. 7, pp. 12, 2013.

[25] D. Owaki, M. Goda, S. Miyazawa, and A. Ishiguro. "A minimal model describing hexapedal interlimb coordination: The tegotae-based approach." Frontiers in Neurorobotics, vol. 11, pp. 29, 2017.

[26] A. Fukuhara, W. Suda, T. Kano, R. Kobayashi, and A. Ishiguro. "Adaptive interlimb coordination mechanism for hexapod locomotion based on active load sensing,'' Frontiers in Neurorobotics, vol. 16, 2022.

[27] V. Dürr, J. Schmitz, and H. Cruse. "Behavior-based modeling of hexapod locomotion: linking biology and technical application," Arthropod Structure and Development, vol. 33, pp. 237–250, 2004.

[28] O. Ekeberg, M. Blümel, A. Büschges. "Dynamic simulation of insect walking," Arthropod Structure and Development,vol.33, pp. 287–300, 2004.

[29] A. von Twickel, A. Büschges, and F. Pasemann, "Deriving neural network controllers from neuro-biological data: implementation of a single-leg stick insect controller." Biological Cybernetics, vol. 104, pp. 95–119, 2011.

[30] M. Schilling, T. Hoinville, J. Schmitz, and H. Cruse. "Walknet, a bio-inspired controller for hexapod walking," Biological Cybernetics, vol. 107, no. 4, pp. 397–419, 2013.

[31] L. Minati, M. Frasca, N. Yoshimura, and Y. Koike. "Versatile Locomotion Control of a Hexapod Robot Using a Hierarchical Network of Nonlinear Oscillator Circuits," IEEE Access, vol.8, pp. 8042–8065, 2018

[32] V. Dürr et al. "Integrative Biomimetics of Autonomous Hexapedal Locomotion," Frontiers in Neurorobotics, vol. 13, 2019.

[33] H. J. Chiel and R. D. Beer. "The brain has a body: adaptive behavior emerges from interactions of nervous system, body and environment," Trends in Neurosciences, vol. 20, no. 12, pp. 553–557, 1997.

[34] R. Pfeifer, M. Lungarella, and F. Iida. "Self-organization, embodiment, and biologically inspired robotics," Science 318.5853, pp. 1088–1093, 2007.

[35] P. Ramdya et al. "Climbing favours the tripod gait over alternative faster insect gaits," Nature Communications, vol. 8, pp. 14494, 2017.

[36] M. Thor et al. "A dung beetle-inspired robotic model and its distributed sensor-driven control for walking and ball rolling," Artificial Life and Robotics, vol. 23, no. 4, pp. 435–443, 2018.

[37] J. Ignasov et al. "Bio-inspired design and movement generation of dung beetle-like legs," Artificial Life and Robotics, vol. 23, no. 4, pp. 555–563, 2018.

[38] D. Shima, J. H. Gan, S. Umezu, and H. Sato. "Smooth and slipless walking mechanism inspired by the open–close cycle of a beetle claw," Bioinspiration and Biomimetics, vol. 16, no. 1, pp. 016011, 2021.

[39] J. Nishii, M. Nagahori, and D. Owaki, "Joint stiffness contributes to hexapod gait stabilization" in Proc. of AMAM2021, 2021.

[40] G. Gabrielli and Th. von Kàrmàn. "What price speed? Specific power required for propulsion of vehicles," Mechanical Engineering, vol. 133, no. 10, pp. 775–781, 1950.

[41] R. Kram, B. Wong, and R.J. Full, "Three-dimensional kinematics and limb kinetic energy of running cockroaches." Journal of Experimental Biology, vol. 200, no. 13, pp. 1919– 1929, 1997.

[42] D. Goldschmidt, F. Hesse, F. Wörgötter, and P. Manoonpong, "Biologically inspired reactive climbing behavior of hexapod robots." in Proc. of 2012 IEEE/RSJ International Conference on Intelligent Robots and Systems (IROS2012), pp. 4632–4637, 2012.

[43] O. Ekeberg and K. Pearson. "Computer simulation of stepping in the hind legs of the cat: an examination of mechanisms regulating the stance-to-swing transition," Journal of Neurophysiology, vol. 94, pp. 4256–4268, 2005.

[44] A. von Twickel, C. Guschlbauer, S.L. Hooper, and A. B.üschges, "Swing velocity profiles of small limbs can arise from transient passive torques of the antagonist muscle alone." Current Biology, vol. 29, no. 1 pp. 1–12, 2019.

[45] T. Akiba, S. Sano, T. Yanase, T. Ohta, and M. Koyama, "Optuna: A Next-generation Hyperparameter Optimization Framework." in Proc. of the 25rd ACM SIGKDD International Conference on Knowledge Discovery and Data Mining, 2019.

[46] E. Todorov, T. Erez, and Y. Tassa, "Mujoco: A physics engine for model-based control." In Proc. of 2012 IEEE/RSJ International Conference on Intelligent Robots and Systems (IROS2012), pp. 5026–5033, 2012.

[47] J. Nishii. "Legged insects select the optimal locomotor pattern based on the energetic cost," Biological Cybernetics, vol. 83, pp. 435–442, 2000.

[48] R. J. Full, R. Blickhan, and L. H. Ting. "Leg design in hexapedal runners," Journal of Experimental Biology, vol. 158, no. 1, pp. 369–390, 1991.

[49] C.J. Dallmann, Düurr, J. Schmitz. "Joint torques in a freely walking insect reveal distinct functions of leg joints in propulsion and posture control," Proceedings of the Royal Society B, vol. 283, no. 1823, pp. 20151708, 2016.